Chinese Chemical Letters 35 (2024) 108669

Contents lists available at ScienceDirect

Chinese Chemical Letters

journal homepage: www.elsevier.com/locate/cclet

Supramolecular flow chemistry: Construction of multiscale supramolecular assemblies by micro/nanofluidic techniques

Leyong Zhou[1], Changyin Yang[1], Weitao Dou*, Tongxia Jin, Haibo Yang, Lin Xu*

Shanghai Key Laboratory of Green Chemistry and Chemical Processes, Shanghai Frontiers Science Center of Molecule Intelligent Syntheses, School of Chemistry and Molecular Engineering, East China Normal University, Shanghai 200062, China

ARTICLE INFO

Article history:
Received 28 February 2023
Revised 6 June 2023
Accepted 7 June 2023
Available online 9 June 2023

Keywords:
Supramolecular chemistry
Self-assembly
Micro/nanofluidics technique
Supramolecular flow chemistry
Supramolecular assemblies

ABSTRACT

The rapid and precise fabrication of multiscale supramolecular assemblies using micro/nanofluidic techniques has emerged as a dynamic area of research in supramolecular chemistry, materials chemistry, and organic chemistry. This review summarizes the application of micro/nanofluidic techniques in constructing supramolecular assemblies, including nanoscale supramolecular assemblies such as macrocycles and cages, microscale supramolecular assemblies such as metal organic frameworks (MOFs) and covalent organic frameworks (COFs), and macroscale supramolecular assemblies such as supramolecular hydrogels. Compared to conventional synthesis methods, micro/nanofluidic techniques for the production of supramolecular assemblies have significant advantages, including enhanced safety, high reaction rates, improved selectivity/yield, and scalability. Additionally, micro/nanofluidic systems facilitate the creation of precisely controllable micro/nanoconfined environments, allowing for a unique flow behavior that improves our understanding of the supramolecular self-assembly process. Such systems may also lead to the development of novel supramolecular assemblies that differ from those generated *via* traditional methods.

1. Introduction

Self-assembly is a process in which individual building blocks spontaneously form well-defined ordered/arranged structures or patterns [1–8] through a variety of noncovalent interactions, including hydrogen bonds, coordination bonds, hydrophilic–hydrophobic interactions, π-π interactions, van der Waals forces, and electrostatic interactions. This process is often driven by thermodynamic principles and the tendency of the components to minimize their free energy and has also been proven to be an important means to developing complex structures and materials with unique properties and functionality at the molecular and nanoscale levels. Hence, massive versatile supramolecular assemblies with well-defined shapes and excellent functions, such as macrocycles [9–11], cages [12–14], metal organic frameworks (MOFs) [15,16], covalent organic frameworks (COFs) [17,18], and supramolecular hydrogels [19,20], have been developed in the past few decades and have a wide range of applications in various classical and emerging fields of sensing [21,22], energy transfer [23–25], gas separation/adsorption [26,27], catalysis [28,29], drug encapsulation/delivery [30,31], medicine [32,33], and electronics [34,35].

Supramolecular assemblies with specific structures and functions often require the careful design of building blocks and precise regulation of the behavior during assembly [36–39]. The synthesis of supramolecular assemblies is relatively straightforward, and there are already well-established synthetic strategies available. However, the self-assembly process occurs in a wide range of systems, from molecular to nanoscale and even at the macroscale in some cases. Typically, the assemblies are obtained by simply placing them in flasks or vials for one-pot assembly after ligand design and preparation. This means that these meticulously assembled substrates are often challenging to fine-tune during assembly, resulting in the final assemblies being largely controlled by spontaneous thermodynamics and making it difficult to achieve nonequilibrium assemblies through kinetic control [40]. It is noteworthy that supramolecular assembly in complex living systems frequently relies on the regulation of individual components on both spatial and temporal scales, facilitating bottom-up synthesis. This suggests that in addition to the careful design of building blocks, a suit-

* Corresponding authors.
E-mail addresses: wtdou@chem.ecnu.edu.cn (W. Dou), lxu@chem.ecnu.edu.cn (L. Xu).
[1] These authors contributed equally to this work.

https://doi.org/10.1016/j.cclet.2023.108669
1001-8417/

able assembly scenario is necessary for precise control over the supramolecular self-assembly process.

Flow chemistry is a technology for the precise manipulation of microfluidics at the microscale, providing a new approach for improving the reaction process and regulating products [41]. Flow chemistry allows the direct control of fluid by adjusting the speed at which the reactants are injected, thus enabling precise control over parameters, such as the reactant ratio and residence time [42,43]. The uniform residence time of reactants in the reaction channel of the flow chemistry platform and reduced backmixing results in improved reaction accuracy [44,45]. Equivalent fluids flowing through the same microchannel position under the same flow conditions allow for *in situ* monitoring of the reaction progress, providing insight into the microscopic reaction mechanism [46,47]. The precise fluid manipulation of the flow chemistry platform combined with the high heat and mass transfer rates of the reactor make it an efficient process intensification technology [48–51].

There are two different microfluidic flow states of flow chemistry platforms: continuous flow and discontinuous flow [52]. In continuous-flow systems, the concentration of reaction substrates can be controlled both temporally and spatially through their diffusion in the microfluidic channels [53,54]. In discontinuous-flow systems, reactants are segregated in a confined environment and mixed more quickly in each droplet [55,56]. To date, flow chemistry has been applied to study various supramolecular assemblies [57–59], such as macrocycles, cages, MOFs, COFs, supramolecular polymers, and supramolecular hydrogels. Flow chemistry has contributed to the development of supramolecular chemistry, for example, by modulating the microscopic morphology of assemblies, promoting assembly efficiency, and allowing the precise control of the component distribution in composites, among other things [60,61]. These contributions facilitate the precise spatial and temporal control of the building blocks in the fluid. Combining supramolecular chemistry with flow chemistry techniques has great potential for developing supramolecular flow chemistry [62], exploiting the advantages of flow chemistry for precise control of chemical reactions, and studying the assembly process and regulating the products of supramolecular chemistry [63].

Supramolecular chemistry is concerned with the study of molecular interactions and the assembly of molecular entities into larger structures [64]. Flow chemistry, on the other hand, is a science and technology that involves the precise manipulation of microfluidics at the microscale for the enhancement of chemical reactions [65]. Based on the above advantages of supramolecular chemistry and flow chemistry, new research directions and fields have emerged, such as "*supramolecular flow chemistry*" named by us, which is defined as "a research field that explores the assembly process, mechanism, precise control, and efficient preparation of supramolecular self-assembly by applying the theories, methods, and techniques of flow chemistry" (Fig. 1). Within this field, a new self-assembly paradigm for the supramolecular self-assembly process was developed and has the potential to provide new insights and perspectives for research on multiple self-assembly events that occur simultaneously through multiple interactions at the molecular scale.

This review aims to summarize the recent developments in the application of flow chemistry in the field of supramolecular chemistry, discuss representative examples of the use of flow chemistry platforms for the specific preparation of supramolecular assemblies and explore how flow chemistry techniques can be utilized to construct nanoscale, microscale, and macroscale supramolecular assemblies. This review provides a comprehensive overview of the research and applications of supramolecular assemblies from the perspective of supramolecular flow chemistry and offers insights and perspectives for future research in this area.

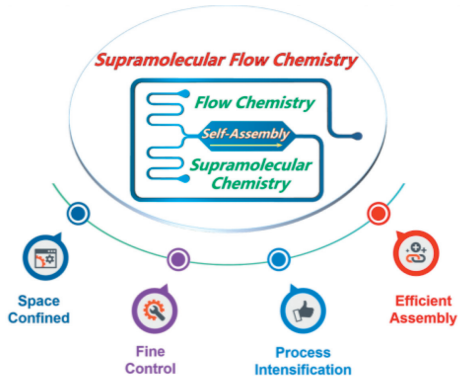

Fig. 1. Schematic diagram of the controllable assembly and effective application of supramolecular assemblies based on supramolecular flow chemistry.

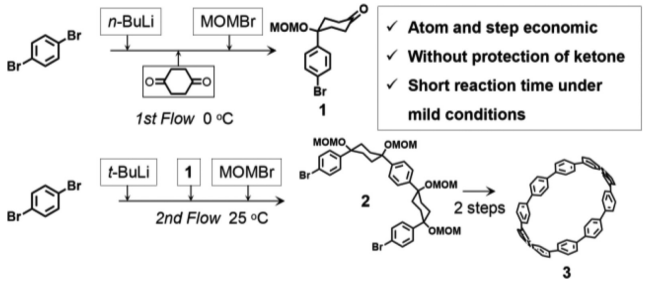

Fig. 2. Micro/nanofluidic technique of an integrated sequential reaction approach for the synthesis of the organic macrocycle [10]CPP in a continuous-flow microreactor. Reproduced with permission [73]. Copyright 2016, Wiley-VCH.

2. Construction of nanoscale supramolecular assemblies by micro/nanofluidic techniques

As representative nanoscale supramolecular assemblies, the development of macrocycles and cages has garnered extensive interest and has been utilized in various areas, such as host-guest recognition [66,67], sensing [68,69], and catalysis [70,71]. Micro/nanofluidic techniques have unique benefits in the design and large-scale synthesis [72] of these nanoscale assemblies, such as covalent macrocycles and cages, due to their high throughput and integrated functionalization. Hence, the synthesis of macrocycles and cages through micro/nanofluidic techniques has received great attention.

In 2016, Kim *et al.* reported the micro/nanofluidic synthesis of the organic macrocycle [10]cycloparaphenylene ([10]CPP, compound **3**), which is widely known as a supramolecular template for the bottom-up synthesis of carbon nanotubes [73]. Traditional synthetic methods for [10]CPP require harsh conditions, such as low temperature (−78 °C), and involve multiple steps, making the synthesis of this molecule extremely time-consuming (approximately 160 h) and labor-intensive. Furthermore, the yield of [10]CPP is relatively low (approximately 5%) when considering the high cost of the process. The nucleophilic reaction of aryl lithium reagents with single diketone sites is difficult to control. Even when the reaction was controlled under harsh conditions of −78 °C, the yield of unilateral nucleophilic reaction products was only 11%, which is far lower (*i.e.*, 26% lower) than that of the bilateral nucleophilic reaction products. In this study, the authors successfully synthesized CPP in only four steps using flow chemistry technology (Fig. 2). The first crucial step was the unilateral Br-Li exchange of 1,4-dibromoaromatics using *n*-butyllithium and the subsequent unilateral nucleophilic reaction of 1,4-dicyclohexanone achieved by rapid mixing under mild conditions (0 °C) within only 3 s. The yield of the intermediate in this step was only slightly reduced, even when

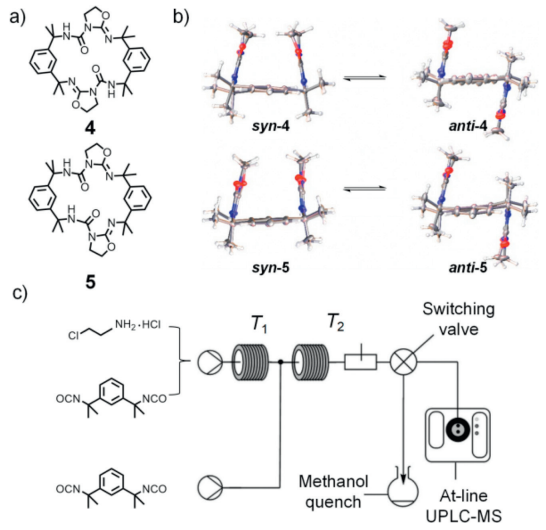

Fig. 3. (a) Chemical structures of two geometric isomer macrocycles **4** and **5**. (b) Crystal structures of macrocycles **4** and **5** in their syn- and antigeometric conformations. (c) Synthesis of macrocycle **5** in the continuous-flow microreactor. Reproduced with permission [74]. Copyright 2021, American Chemical Society.

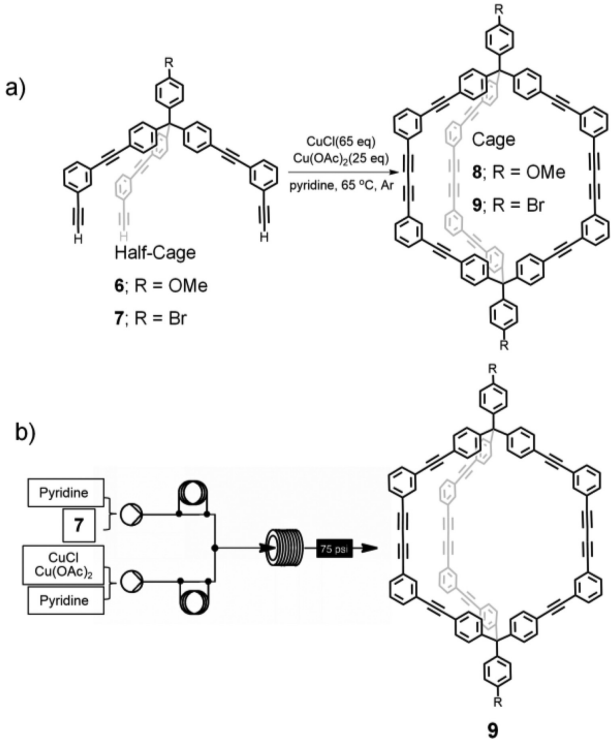

Fig. 4. (a) Traditional batch synthesis of organic cage **9**. (b) Synthesis of organic cage **9** in a continuous-flow microreactor. Reproduced with permission [77]. Copyright 2015, The Royal Society of Chemistry.

the reaction was performed at room temperature. Subsequently, bromomethyl methyl ether (MOMBr) was introduced into the flow chemistry system, and the effluent fluid was collected in a vial and then stirred for 4 h to obtain compound **1**. The second critical step was the mixing of *n*-butyllithium with 1,4-dibromobenzene in a flow chemistry system at 0 °C for 20.9 s to allow complete double Br-Li exchange of 1,4-dibromobenzene. Next, compound **1** was introduced into the flow chemistry system and mixed with this aryl lithium compound for 63 s. Then, MOMBr was introduced into the flow chemistry system, which was allowed to continuous flow with the previous fluid mixture for 50 s. The key intermediate compound **2** of [10]CPP was obtained in 68% yield by collecting the fluid at the outlet. Finally, compound **2** was converted to complete [10]CPP by two steps of cyclic dimerization and aromatization.

The separation of isomers of covalent macrocycles with geometric conformations in flask reactions is frequently challenging. In 2021, Slater and coworkers reported the synthesis of two isomeric macrocycles, compounds **4** and **5**, which exhibited clamp-like open and closed geometric conformations (Fig. 3a) [74]. The macrocycles anti-**4** and syn-**5** were achiral, while the macrocycles syn-**4** and anti-**5** were chiral, and all four isomers had racemic crystal forms that were difficult to separate (Fig. 3b). Micro/nanofluidic techniques enabled the selective continuous synthesis of macrocycle **5** by precisely controlling the stoichiometric ratio and reaction temperature, eliminating the need for a separation process. Compared to traditional methods, the synthesis was simpler and resulted in fewer byproducts. Combining NMR and HPLC–MS studies, it was determined that an increase in temperature reduced the production of intermediates and improved reaction efficiency. As a result, this research successfully achieved continuous-flow synthesis of the organic macrocycle with high conversion rates of 85%–93% and over 80% selectivity for the single isomer, macrocycle **5** (Fig. 3c).

Organic cages are considered to be another significant type of nanoscale supramolecular assembly [75]. However, the synthesis of organic cages is usually affected by local concentration [76]; thus, it is difficult to achieve rapid and large-scale synthesis. The advent of micro/nanofluidic techniques offers a promising approach for the synthesis of organic cages on a large scale. In 2015, Doonan and colleagues reported the synthesis of organic cage **9** in a micro/nanofluidic reactor [77]. In their previous work, the authors successfully synthesized cage **8** and **9** from compounds **6** and **7** using copper-catalyzed coupling reactions in a conventional flask reaction mode. For the traditional flask reaction, excessive amounts of copper coupling reagents were required, resulting in a yield of only 20% (Fig. 4a). Using a micro/nanofluidic reactor (Fig. 4b), the synthesis of the organic cage was improved, with the reactor providing efficient support for mass and heat transfer, as well as enhancing reaction speed and safety. The use of micro/nanofluidics reduced the consumption of copper coupling catalysts $Cu(OAc)_2$ and CuCl by 68% and 29%, respectively, compared to traditional flask reactions. With an optimal flow rate of 0.6 mL/min and a reaction temperature of 70 °C, the reaction rate in the micro/nanofluidic reactor was significantly faster, yielding the target compound in 21% yield in only 33.3 min, which is 99.3% shorter than the conventional reaction. These results demonstrate that the use of micro/nanofluidic techniques is an efficient method for the large-scale synthesis of organic cages.

In the same year, Cooper and coworkers reported the rapid synthesis of two imine-based organic cages (CC1 and CC3) in a micro/nanofluidic reactor [78]. The preparation of organic cage CC3 involved dissolving 1,3,5-triformylbenzene (TFB) and 1,2-cyclohexanediamine (CHDA) in dichloromethane (DCM). The stoichiometry was controlled by mixing TFB and CHDA in a 4:6 ratio before injecting it into the flow reactor (Fig. 5a). The optimal conditions for the synthesis of CC3-R in the micro/nanofluidic reactor were determined to be a flow rate of 0.62 mL/min for CHDA and 0.38 mL/min for TFB, a reaction time of 10 min, and a temperature of 100 °C (Fig. 5b). The micro/nanofluidic reactor was also suitable for the rapid synthesis of organic cage CC1, which was achieved by changing the amine ligand to ethylenediamine (EDA) and replacing the solvent DCM with a mixed solvent of methanol/DCM (1:3).

The results of HPLC analysis indicated that the purity of the organic cages CC1 and CC3-R synthesized using the micro/nanofluidic reactor was maintained at greater than 99%, while the reac-

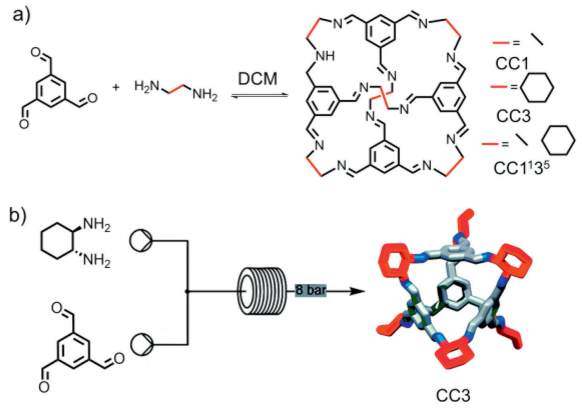

Fig. 5. (a) Traditional batch synthesis of organic cages (CC1 and CC3). (b) Synthesis of an organic cage (CC3) in a continuous-flow microreactor. Reproduced with permission [78]. Copyright 2015, The Royal Society of Chemistry.

tion time was significantly reduced. Utilizing a single 10 mL micro/nanofluidic reactor, the synthesis and separation efficiency of CC1 was 0.35 g/h, with a yield of 93%, and that of CC3 was 0.50 g/h, with a yield of 95%. In comparison, the traditional flask reaction required 3–5 days and had a yield of 94% for CC1 and 83% for CC3. The application of micro/nanofluidic technology facilitated the reduction in reaction time due to the heating of DCM to 100 °C within the micro/nanofluidic reactor, which greatly improved the effect of mass and heat transfer.

3. Construction of microscale supramolecular assemblies by micro/nanofluidic techniques

Supramolecular assemblies on the microscale, with two of the most well-known examples being MOFs and COFs, are typically formed by the self-assembly of small subnanometer molecules with long-range ordered arrangements. These materials belong to a class of porous crystalline substances that exhibit exceptional performance in adsorption [79,80], separation [81,82], and catalysis [83,84] as a result of their multidimensional network structures with periodic arrangements. The most widely used methods for the batch synthesis of MOFs and COFs are hydrothermal and solvothermal techniques [85,86]. However, these processes often require several hours to multiple days of reaction time, making them time- and energy-intensive, and it is challenging to control the product morphology. This leads to difficulties in the large-scale production of these materials.

The microchannels of flow chemistry platforms possess a high specific surface area and heat and mass transfer efficiency, which make them a powerful tool for enhancing microscopic reaction processes and improving reaction efficiency. Additionally, several flow chemistry platforms have been developed to facilitate the microscopic control of synthesis processes, allowing the rapid preparation of supramolecular functional materials with varying morphologies. It is also possible to produce precisely and controllably monodisperse micron-sized supramolecular assemblies through flow chemistry, such as some supramolecular copolymers [87].

In flow chemistry, there are two distinct microfluidic flow states: continuous flow and discontinuous flow. The discontinuous-flow state is further categorized into droplet flow and slug flow. The internal convection within the droplet flow state can enhance the mixing efficiency, thereby facilitating rapid mixing of the liquids inside the droplet, which promotes the reaction. In 2013, Faustini and colleagues reported the synthesis of various carboxylate MOF materials, including HKUST-1, MOF-5, IRMOF-3, and UiO-66, utilizing droplet microfluidic devices (Fig. 6a) [88]. A T-junction

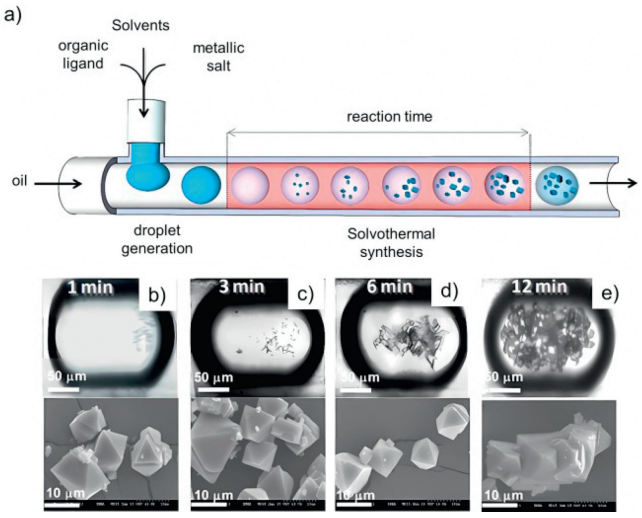

Fig. 6. (a) Schematic representation of the general microchemical process. Optical and scanning electron microscopy (SEM) images of HKUST-1 crystals synthesized through the microfluidic approach after (b) 1, (c) 3, (d) 6, and (e) 12 min of synthesis. Reproduced with permission [88]. Copyright 2013, American Chemical Society.

polydimethylsiloxane (PDMS) chip was fabricated using a template method, and a polar medium solution of organic and metal precursors was employed as the dispersed phase, while silicone oil served as the continuous phase. This process generated discrete nanoliter droplets, which were then transported to the perfluoroalkoxyalkane (PFA) tube attached to the chip, serving as the reaction site for the MOF synthesis. The reaction time was adjusted between 1 and 15 min by controlling the fluid flow rate in the chip, while the reaction temperature was controlled by placing the PFA tube in an oil bath or oven (Figs. 6b–e). The confined precursor solutions in individual nanoliter droplets rapidly mixed due to the chaotic advection of the fluid, and the high specific surface area of the confined environment enhanced heat and mass transfer, leading to rapid crystalline MOF preparation.

Compared to the traditional solvothermal method, which requires 20 h at 85 °C, the flow chemistry system allowed the precursor solution to react at 90 °C for 1 min, yielding visible crystal particles (Fig. 6b). The product yield reached 68% after 12 min, equivalent to the yield of the conventional batch synthesis after 24 h (Figs. 6c–e). The space-time production rate was approximately 5.8 kg/m^3 per day, 5–6 times greater than that of traditional synthetic methods. Product characterization revealed that the microfluidic product and the bulk reaction product had the same morphology, composed of typical 5–15 μm octahedral crystals with the same crystal structure. The flow chemistry method was also used to synthesize MOF-5 and IRMOF-3 by reacting at 120 °C for 3 min and UiO-66 by reacting at 140 °C for 15 min. The authors also used this method to rapidly prepare $Ru_3(BTC)_2$ crystals, which typically require harsh high-pressure hydrothermal synthesis conditions. Additionally, the authors innovatively synthesized heterostructured MOF crystals composed of core-shell or magnetic core-MOF shell composites *via* a two-step serial microfluidic approach.

In the same year, Coronas and his colleagues reported the synthesis of a series of MIL-88B-type MOFs using the slug flow approach [89]. As shown in Fig. 7, a flow chemistry platform with a double Y-shaped structure was designed and fabricated for this purpose. The metal solution and the ligand solution were separately injected into the first Y-shaped structure, followed by the mixing of these solutions within this structure and the transmission of the mixed solution to one of the injection ports of the second Y-shaped structure. Simultaneously, silicone oil was intro-

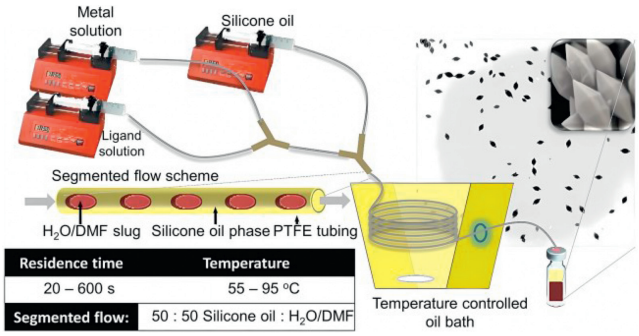

Fig. 7. Schematic illustration of the microfluidic setup, segmented flow pattern, and synthesis details. The flow rates of both reactants and silicone oil were maintained at equal values within the range of 60–600 μL/min, resulting in residence times ranging from 20 s to 600 s. Reproduced with permission [89]. Copyright 2013, American Chemical Society.

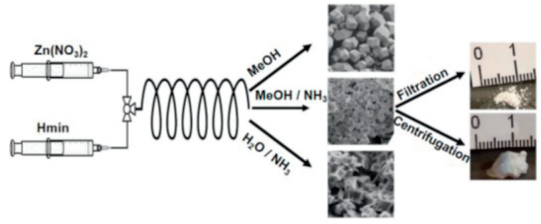

Fig. 8. Schematic illustration of the process used for the continuous synthesis of ZIF-8. Reproduced with permission [90]. Copyright 2016, Elsevier Ltd.

duced into another injection port of the second Y-shaped structure as the continuous phase to generate slug flow. The slug flow was then conveyed to a helical Teflon tube, where the reaction took place. This flow chemistry platform enabled the ultrafast synthesis of three MIL-88B-type MOFs (Fe-MIL-88B-NH_2, Fe-MIL-88B and Fe-MIL-88B-Br) at 95 °C, although the yields were lower than those reported in other studies. Additionally, the residence time of the microfluid in the platform was controlled by regulating the flow rate of the fluid. The longer the residence time was, the larger the volume of slug flow formed. Under segmented flow, the fluid inside the segmented plug underwent internal circulation, determined by the flow velocities of the continuous and discontinuous phases and the volume of the segmented plug. This internal annular flow had a direct impact on the particle size distribution of the crystals, allowing control of the crystal size of MOFs in the range of 90–900 nm.

In comparison to the discontinuous-flow state, the continuous-flow state does not have a discontinuous phase fluid occupying the channel space of the flow chemistry platform, thus resulting in a higher spatiotemporal yield. In 2016, Polyzoidis and his colleagues reported the synthesis of the zeolitic imidazolate framework-8 (ZIF-8) through continuous-flow chemistry (Fig. 8) [90]. The researchers utilized a T-shaped structure by connecting capillaries to create a flow chemistry platform and introduced two types of precursor solutions (a $Zn(NO_3)_2{\cdot}6H_2O$ solution and a 2-methylimidazole (Hmim) solution) into the T-shaped micromixer using two syringe pumps. The mixed precursor solutions were then transported to a helically wound capillary reactor connected to the mixer where they reacted at room temperature. The morphology of the resultant ZIF-8 (both microscopic and macroscopic) was regulated by controlling the reaction time, reaction solvent system, and postprocessing methods. When pure methanol was used as the reaction solvent, the reaction proceeded at a slow rate, and the yield was low, reaching only 3% to 10%. However, as reported by Zhang *et al.*, the synthesis of ZIF-8 by dissolving the Zn precursor in ammonia was found to be a feasible solution to the slow reaction rate and low yield observed when using MeOH as a single solvent. When using MeOH/NH_3 (aq) as the reaction solvent, the production capacity of this flow chemistry platform increased to 30–640 g/day, which corresponded to theoretical space-time yields ranging from approximately 10,000–210,000 kg/m^3 per day, several orders of magnitude higher than most theoretical space-time yields reported for ZIF-8.

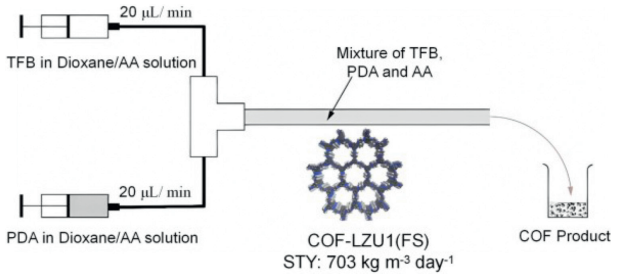

Fig. 9. Schematic illustration of the continuous flow synthesis of COF-LZU1 (FS). Reproduced with permission [91]. Copyright 2016, American Chemical Society.

In 2016, Zhao and colleagues reported the first example of synthesizing COFs through continuous-flow chemistry (Fig. 9) [91]. The reaction precursor solution was obtained by using the room temperature solution-suspension approach, and three 2D COFs (COF-LZU1, TpPa-1, and N3-COF) were synthesized in batch form over the course of three days at room temperature. These COFs were found to have higher crystallinity and specific surface areas compared to COFs synthesized through the solvothermal synthesis method, which requires elevated temperatures. This room-temperature batch synthesis method was facilitated by two main factors: (1) the high solubility of the monomers and (2) the strong π-π interaction between the monomers and oligomers, which played a crucial role in promoting the crystallization of the product. Based on this work, the researchers subsequently developed a continuous and rapid synthesis method for COF-LZU1 in a flow chemistry device. Stock solutions of 1,3,5-triformylbenzene (TFB) and *p*-phenylenediamine (PDA) were prepared and combined in a flow reactor, where they were mixed in a T-type micromixer and reacted within 11 s. Despite the short reaction time, the theoretical space-time yield was as high as 703 kg/m^3 per day. The resulting COF-LZU1 synthesized through flow chemistry exhibited a higher Brunauer–Emmett–Teller (BET) surface area than the batch-synthesized COF-LZU1, possibly due to the improved crystallization process facilitated by high local supersaturation at the interface between the two flows.

In addition to the aforementioned instances of microscale supramolecular assembly synthesis using flow chemistry, numerous other cases have been documented in recent years. All of these cases demonstrate the exceptional benefits of utilizing the flow chemistry platform for the rapid synthesis of MOF and COF materials. For a comprehensive review on this topic, please refer to the following papers [92–94].

Morphology modulation in flow chemistry platforms is typically achieved through phase interface control in microfluidics or the rational design of microchannels. In discontinuous flow, the phase interface of the droplet provides an ideal support for controlling the assembly of the building blocks, which holds promise for the precise control of MOF and COF morphologies. Hence, the utilization of flow chemistry has demonstrated potential for the rapid and precise synthesis of MOFs and COFs.

In 2011, De Vos and his colleagues employed a discontinuous-flow chemistry platform to synthesize dense microcrystalline hollow capsules of MOFs (Fig. 10a) [95]. The process involved dissolving metal ions in water and organic ligands in octanol. The organic phase was then added to the aqueous phase, leading to the nucle-

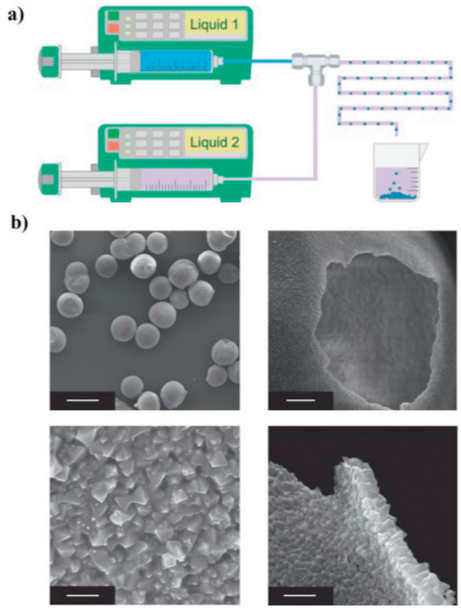

Fig. 10. (a) Schematic illustration of the droplet flow synthesis of $[Cu_3(BTC)_2]$ capsules. (b) SEM images of hollow $[Cu_3(BTC)_2]$ capsules; all images have a scale bar of 2 μm. Reproduced with permission [95]. Copyright 2011, Springer Nature.

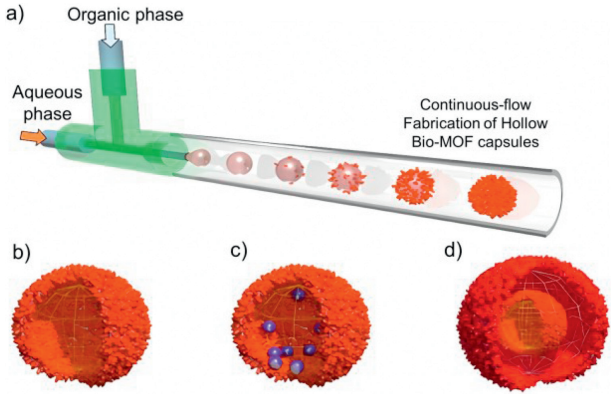

Fig. 11. (a) Schematic of the synthesis of hollow MIL-88A MOF architectures through a microfluidic approach. A dispersion of an aqueous phase of the metal precursor solution and a continuous oil phase of the organic linker are introduced into a microfluidic channel through a T-junction. (b) MIL-88A hollow spheres with a single shell structure. (c) Single-shell MIL-88A hollow spheres encapsulating functional components. (d) MIL-88A spheres with a double-shell structure. Reproduced with permission [96]. Copyright 2015, American Chemical Society.

ation and growth of $[Cu_3(BTC)_2]$ MOFs through a copper-center ligand exchange mechanism. A 2D MOF film was obtained by simply letting the mixture stand at room temperature. In a flow chemistry platform with a T-shaped structure, the metal ion solution was injected into one of the ports as the dispersed phase, while the octanol solution of the organic ligand was injected into the other port as the continuous phase. The shearing force generated microdroplets of water-in-oil (W/O) that took the shape of the liquid–liquid interface. This enabled the formation of three-dimensional MOF objects. As the microdroplets flowed through the reaction tube, the planar shape of the polymerization interface transformed into a spherical shape, resulting in $[Cu_3(BTC)_2]$ capsules with a 3D hollow film structure (Fig. 10b).

The reaction time of MOFs at the phase interface was controlled by adjusting the length of the reaction tubes, while the size of the microdroplets was regulated by modulating the flow rate ratio between the organic phase and the aqueous phase, leading to the production of MOF capsules with varying hollow morphologies. The use of more reactive copper acetate in place of copper nitrate as the reaction precursor and the adjustment of the aqueous and oil phase solutions to near saturation conditions increased the reaction rate and resulted in the rapid synthesis of hollow MOF capsules. The addition of 1–3 wt% polyvinyl alcohol (PVA) to the aqueous phase prevented droplet fusion and significantly improved the mechanical stability of the capsules. Selective permeation experiments indicated that the surface pore structure of $[Cu_3(BTC)_2]$ capsules allowed for the permeation of small ethylene glycol molecules, while larger rose bengal (RB) molecules were retained inside the capsules. These results suggest that MOF capsules are promising candidates for application in selective microreactors.

In 2015, Falcaro *et al.* successfully synthesized hollow MIL-88A capsules utilizing the microdroplet phase interface of a flow chemistry platform (Fig. 11) [96]. The size of the capsules was modulated by adjusting the flow ratio of the dispersed phase, continuous phase, and reaction tube diameter. Magnetic particles, silica nanoparticles, UiO-66 nanoparticles, and biological enzymes were introduced into the hollow core of the capsules by modifying the composition of the dispersed phase, which allowed the MOF capsules to have distinct properties and various potential applications, such as biomass conversion, biosensing, and biopharmaceuticals. Moreover, double-shell MIL-88A capsules were produced by generating O/W/O multiple microdroplets through tandem microfluidic chips, enabling further control of the microstructural diversity of the MOF capsules.

In 2019, Sun *et al.* developed a droplet microfluidic synthesis method for the continuous preparation of MOF capsules with a hierarchical pore structure at the phase interface of the droplet within a few minutes (Fig. 12) [97]. The formation of this structure was attributed to the growth process of the MOF capsules following the reaction/diffusion principle. After the rapid formation of dense MOF capsules, the assembly elements diffused through the membrane to generate bilayer MOF capsules with a smooth inner surface and a large number of porous microstructures on the outer surface. Additionally, the size of the MOF hollow capsules was precisely controlled by regulating the relative flow rates of the organic and aqueous phases. The dense layer within the double-layer structure capsule tightly encapsulated magnetic particles, while the outer porous structure supported Au nanoparticles. Finally, as a heterogeneous catalyst, this MOF exhibited exceptional catalytic and recycling performance in catalytic reactions.

Fluid flows containing different assembly components that intersect in the microfluidic chip allow control of the morphology of the assembly by laminar diffusion between the interfaces. Previous studies showed that MOFs coated on the outside of enzymes can be used to enhance enzyme stability, but the dense MOF shell reduced the enzyme activity due to poor mass transfer efficiency and limited contact between the enzyme and substrate (Figs. 13a and b) [98]. To resolve this issue, Ge *et al.* employed microfluidic technology to prepare enzyme–MOF composites with crystal defects. In this study, Zn^{2+}, 2-MeIM, and enzymes were configured into corresponding solutions, which were injected into a double Y-shaped microfluidic chip, mixed *via* the interfacial diffusion mechanism and synthesized in the microchannel. Powder X-ray diffraction (PXRD) (Fig. 13c) showed that the microfluidically prepared enzyme-MOF composites had lower crystallinity than the bulk solution-synthesized composites and pure MOFs. The reason for this was that interfacial diffusion mixing produced radial concentration gradients at the interface, resulting in defects in the MOF crystal structure. The enzyme–MOF complexes prepared by three representative feeding sequences using microfluidic chips showed significantly higher activity than those prepared by bulk solution synthesis, and the complexes prepared by preferentially

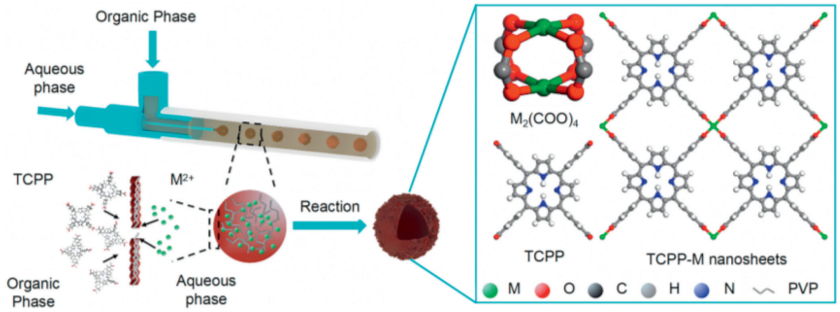

Fig. 12. Schematic representation of the fabrication and structure of hierarchical MOF nanosheet microcapsules (HMNMs) prepared with a droplet microfluidic strategy. Reproduced with permission [97]. Copyright 2019, Springer Nature.

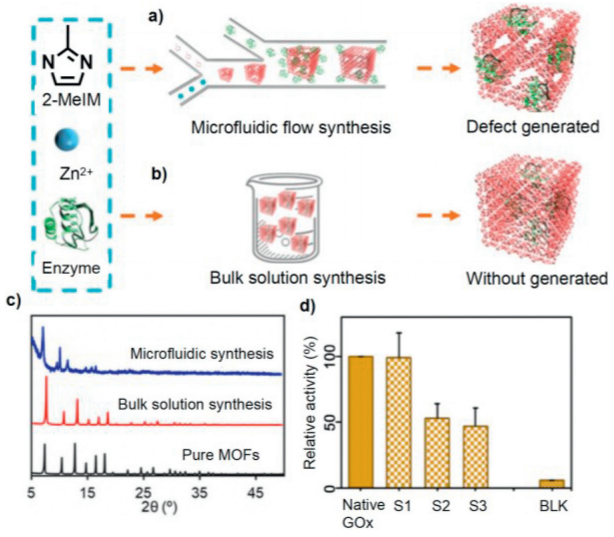

Fig. 13. (a, b) Schematics of the enzyme–MOF composites fabricated by microfluidic flow synthesis and bulk solution synthesis. (c) PXRD patterns of microfluidic- and bulk solution-synthesized composites and pure MOFs. (d) Relative enzymatic activity; Native GOx: native glucose oxidase; S1: The MOF complex with the enzyme obtained by injecting 2-MeIM and Zn^{2+} in the first Y-shaped channel and subsequently passing the enzyme in the third injection port; S2: The MOF complex with the enzyme obtained by injecting enzyme and Zn^{2+} in the first Y-shaped channel and subsequently passing the 2-MeIM in the third injection port; S3: The MOF complex with the enzyme obtained by injecting 2-MeIM and Zn^{2+} in the first Y-shaped channel and subsequently passing the enzyme in the third injection port; BLK: blank solution. Reproduced with permission [98]. Copyright 2020, American Association for the Advancement of Science.

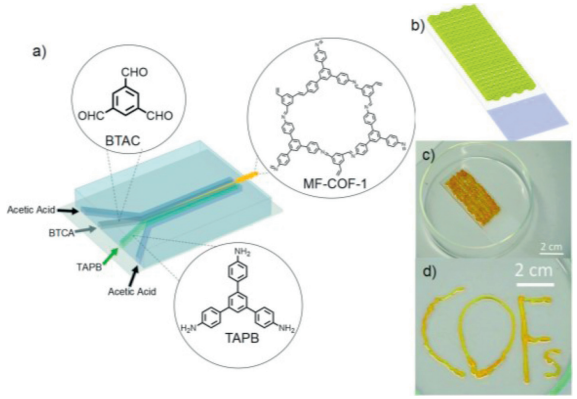

Fig. 14. (a) Schematic representation of the microfluidic synthesis of MF-COF-1. (b) Schematic illustration and (c) micrograph of the 3D MF-COF-1 network printed on glass. (d) Printed word "COFs". Reproduced with permission [100]. Copyright 2016, The Royal Society of Chemistry.

mixing zinc ions (Zn^{2+}) and 2-MeIM demonstrated the same activity as the native enzyme (Fig. 13d). This suggests that the crystal structure defects caused by the reduced crystallinity improved the mass transfer efficiency, making the enzyme substrate more accessible and reducing the impact of MOFs on the enzyme activity.

COFs have demonstrated significant potential for applications in diverse fields, such as adsorption, photocatalysis, CO_2 reduction, supercapacitors, and fuel cells [99]. However, the strong π-π interactions between their molecular layers often lead to structural stacking and the concealment of active sites. This reduces the ability of substrates to interact with active sites, ultimately compromising the material properties. One effective strategy for addressing this issue is the use of phase-controlled interfacial synthesis through continuous-flow chemistry. In 2015, Puigmarti-Luis and colleagues reported the synthesis of MF-COF-1 using a four-inlet flow chemistry microreactor based on a phase interface (Fig. 14a) [100]. Acetic acid solutions of 1,3,5-tris (4-aminophenyl) benzene and trimesic aldehyde were injected into the microfluidic chip, along with pure acetic acid solutions. The resulting merging of the four-phase fluids led to interface formation. The presence of acetic acid in the reaction rendered it highly reversible and facilitated the dynamic chemical conditions necessary for the self-healing of accidental defects during COF formation. This approach made it possible to improve COF crystallinity by controlling the dynamic mixing of assembly elements. The reaction time was only approximately 11 s, which was sufficient for the formation of tiny fibrous crystals at the phase interface. The fibrous crystalline cross-connections formed sponge-like products that were mechanically stable and enabled the direct drawing of simple objects on solid surfaces (Figs. 14b–d).

The refinement of the design of the microfluidic chip itself also has a positive effect on the preparation of microscale supramolecular assemblies with controllable microstructures. In 2012, Lammertyn *et al.* developed a high-throughput, automated method for synthesizing HKUST-1 crystals by combining droplet-based flow chemistry with electrowetting (Fig. 15) [101]. This work presented a microfluidic approach for precisely depositing monodisperse single MOF crystals, enabling efficient, flexible, and high-throughput single-crystal patterning. A novel microfluidic chip consisting of a modular two-piece digital microfluidic device was designed, in which the bottom plate contained electronics specifically designed for transporting micro- to nanoliter-sized "mother droplets". The detachable top plate contained hydrophilic-in-hydrophobic micropatches tailored to print femtoliter-size droplets. As the mother droplet was transported over the hydrophilic-in-hydrophobic micropatches, the femtoliter droplets were selectively partitioned within the hydrophilic regions due to their preferential wetting behavior. The top plate was then removed, and the solvent was slowly evaporated to form HKUST-1 monodisperse single octa-

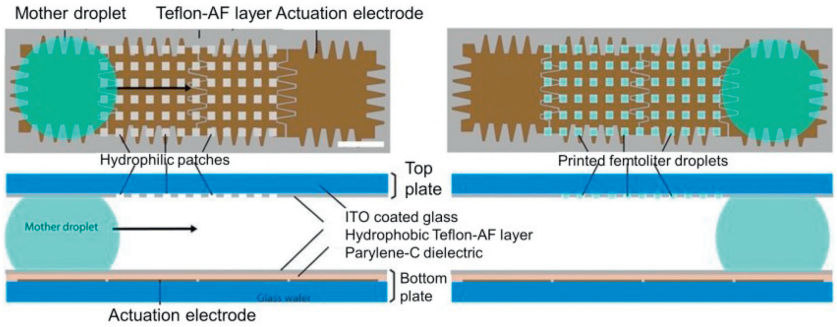

Fig. 15. Schematic diagram of the modular two-piece digital microfluidic device and digital microfluidics scheme. Reproduced with permission [101]. Copyright 2012, Wiley-VCH.

hedral crystal crystallites with a size of $5.3 \pm 0.9\,\mu m$ on the hydrophilic lattice. Typically, only one crystal formed in each hydrophilic lattice, and the formation of a second crystal was rare. The authors also employed this technique to prepare HKUST-1 thin films by controlling the reaction of the mother liquor to flow through the hydrophilic lattice many times, enabling layer-by-layer self-assembly on the lattice.

4. Construction of macroscale supramolecular assemblies by micro/nanofluidic techniques

In general, macroscopic supramolecular assemblies are typically characterized by their large size and visible structure [102]. They can be observed without the aid of a microscope or other magnification tools. Conversely, microfluidics is a technique utilized for the precise manipulation of fluids at the microscale [103], which refers to a size range that is typically at least an order of magnitude smaller than that of macroscale supramolecular assemblies. As a result, direct control of macroscale supramolecular assemblies using microfluidics can be challenging due to the considerable differences in their dimensions [104]. Despite this challenge, scientists have attempted to construct macroscale supramolecular assemblies utilizing a bottom-up approach based on the controllability and stability of microfluidics. Additionally, the rational design of microfluidic chips can enable the coating of smaller-scale supramolecular assemblies directly on substrates [105], thus enabling the macroscopic integration of microscale supramolecular assemblies.

Supramolecular hydrogels represent a significant class of supramolecular assemblies that have garnered considerable research attention due to their precise assembly and diverse application potential [106,107]. These hydrogels are formed through non-covalent interactions, including hydrogen bonds, electrostatic interactions, host-guest interactions, coordination bonds, and dynamic-covalent bonds, between soluble building blocks [108]. The resulting complex network structure immobilizes substantial quantities of water and solvents, thereby enabling wide-ranging applications across various fields, including catalysis [109,110], drug delivery [32,111], and self-healing materials [112,113].

However, traditional batch reactions for constructing supramolecular hydrogels have limited precision in controlling cross-linking reactions and macroscale structures. In recent years, droplet-based micro/nanofluidic techniques have emerged as a high-throughput method for assembling supramolecular hydrogels with precisely controlled composition, size, and shape [114,115]. These techniques enable discrete droplet reactors to assemble supramolecular hydrogels [116], and a common strategy is the preparation of zero-dimensional supramolecular hydrogel microspheres using discontinuous flow. These microspheres, which are more uniform in composition than macroscale supramolecules,

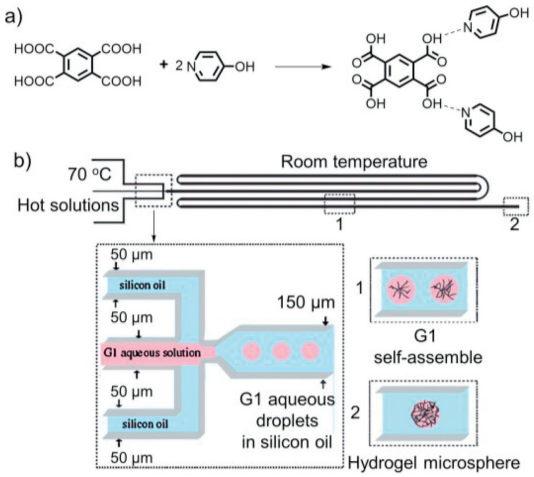

Fig. 16. (a) Synthetic route of a supramolecular hydrogel *via* self-assembly of BTA and PHP. (b) Schematic representation of the self-assembly of supramolecular hydrogel in a droplet-based micro/nanofluidic system [119]. Copyright 2009, American Chemical Society.

can be considered the products of the disassembly of macroscale supramolecules [117]. They can be further assembled into macroscopic supramolecular hydrogel assemblies on demand, representing a new bottom-up approach for constructing macroscale supramolecular assemblies [118]. In this section, we will first discuss the application of flow chemistry techniques to precisely construct zero-dimensional supramolecular hydrogels, which can subsequently be used to create macroscale supramolecular assemblies with various dimensions.

In 2009, Shen *et al.* reported the formation of zero-dimensional supramolecular hydrogel microspheres using a droplet-based micro/nanofluidic system [119]. They employed 1,2,4,5-benzene tetracarboxylic acid (BTA) and 4–hydroxy pyridine (PHP) as building blocks to self-assemble supramolecular hydrogels *via* hydrogen bonds (Fig. 16a). The traditional flask reaction method involves completely dissolving BTA and PHP in an aqueous solution at 90 °C, which is then allowed to self-assemble into a supramolecular hydrogel upon cooling to room temperature. However, this method does not allow control over the size and shape of the resulting supramolecular hydrogel. In contrast, to address this issue, the authors utilized micro/nanofluidic droplet techniques to fabricate supramolecular hydrogel microspheres with uniform size. As shown in Fig. 16b, they injected the aqueous solution of supramolecular hydrogels as the dispersed phase and silicon oil as the continuous phase into a T-shaped PDMS chip microchannel. The self-assembly process of supramolecular hydrogels occurred when the droplet temperature was below 64 °C. After the droplet

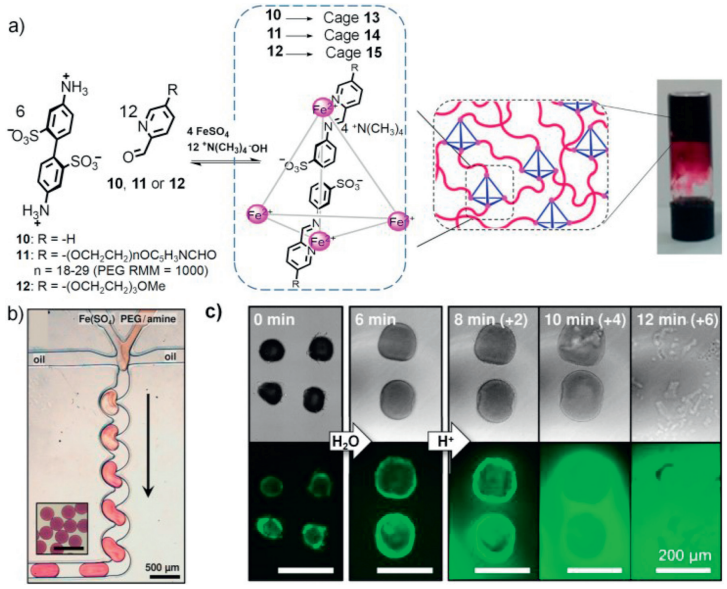

Fig. 17. (a) Schematic diagram of the formation of supramolecular hydrogels *via* conidiation-driven self-assembly. (b) Digital photograph of a droplet-based micro/nanofluidic device for forming microdroplets. (c) TEM (top) and fluorescence (bottom) images of supramolecular hydrogels for releasing guests. Reproduced with permission [120]. Copyright 2015, American Chemical Society.

temperature cooled to room temperature in the chip channel, the supramolecular hydrogel began to solidify and form microspheres. By varying the flow rates, uniform supramolecular hydrogel microspheres with adjustable sizes were obtained.

In 2015, Nitschke and colleagues reported a novel class of supramolecular hydrogels constructed through cross-linked polymers using subcomponent blocks of supramolecular metal-organic cages [120]. These supramolecular metal-organic cages had excellent host-guest properties, selectively encapsulated guest molecules and were assembled directly from starting reagents in water under mild conditions [13]. The authors first synthesized cages **13**, **14**, **15** in vials using different subcomponent blocks (**10**, **11**, **12**), wherein solely cage **14** exhibited the characteristics of the hydrogel. Based on this result, a droplet-based micro/nanofluidic technique was employed to fabricate supramolecular hydrogel microparticles.

The researchers introduced cross-linking sites on the vertices of supramolecular metal-organic cages to form supramolecular hydrogels (Fig. 17a). Based on the host-guest properties of the cage, the porosity of this supramolecular hydrogel had the ability to continuously trap and release guest molecules. They investigated the properties of the supramolecular hydrogels in the droplet-based micro/nanofluidic device, which produced microdroplets to form highly monodisperse supramolecular hydrogel microparticles with a uniform composition (Fig. 17b).

The micro/nanofluidic system, combined with transmission and fluorescence microscopy, was employed to image the microparticles, enabling the observation of supramolecular hydrogel behavior, stimuli-responsive properties, and guest release. Six minutes after water was added, the volume of the supramolecular hydrogel microparticles was increased to several times the original volume, but their structure remained intact, and only a small amount of guest molecule was lost. After adding 0.1 mol/L *p*-toluenesulfonic acid, the supramolecular hydrogel microparticles gradually disassembled, the guest was released continuously for 2 min, and the microspheres were completely disassembled after 12 min (Fig. 17c). This research suggests that the preparation of supramolecular hydrogel microparticles with molecular delivery by micro/nanofluidic techniques holds great potential for drug delivery applications.

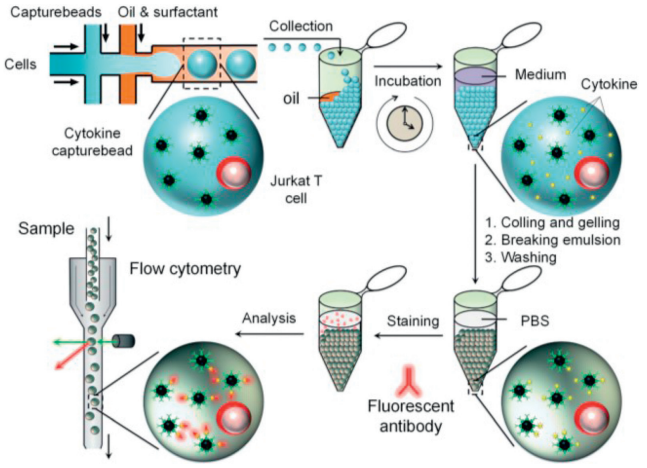

Fig. 18. Schematic of single-cell encapsulation and the detection of secreted cytokines using supramolecular agarose hydrogel droplets in a droplet-based micro/nanofluidic system. Reproduced with permission [123]. Copyright 2013, The Royal Society of Chemistry.

Furthermore, microvesicular structures composed of supramolecular hydrogels have been widely utilized as micro/nanoreactors for high-throughput single-molecule/cell encapsulation and detection in droplet-based micro/nanofluidic systems [121]. In particular, single-cell analysis based on micro/nanofluidic systems has a wide range of potential applications [122], but there are also many challenges, such as the difficulty in culturing cells on a chip, the limited size of cells due to the size of the chip channel, and the greater investment required for micro/nanofluidic techniques. In 2013, Huck and coworkers used supramolecular agarose hydrogel droplets to analyze the secreted cytokines, interleukin-2 (IL-2), rHuIFN-γ (IFN-γ) and tumor necrosis factor-α (TNF-α) of cancer cells in a micro/nanofluidic system [123]. As shown in Fig. 18, a T-shaped PDMS chip was designed, with two injection ports for supramolecular agarose hydrogel aqueous solution as the dispersed phase and another injection port for the cell solution, and oil was used as the continuous phase. Cancer

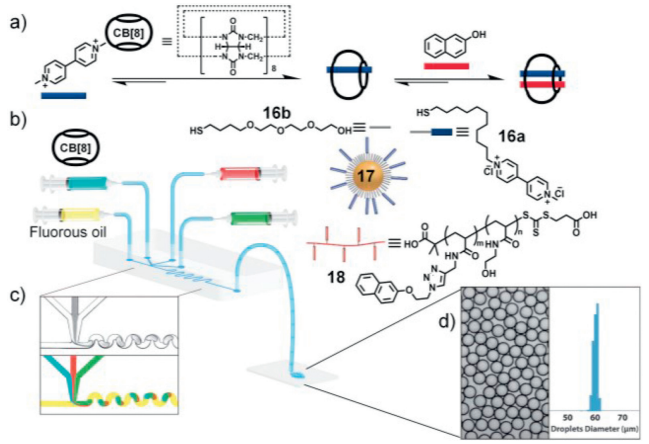

Fig. 19. (a) The two-step, three-component formation of the CB[8] ternary complex in water with MV^{2+} (blue) and Np (naphthalene) (red). (b) Schematic representation of the microdroplet generation process using a microfluidic T-junction device, consisting of an continuous oil phase perpendicular to a combination of three aqueous solutions of CB[8], **17** (AuNP functionalized with a mixture of neutral and viologen-containing ligands **16a** and **16b**), and **18** (copolymer functionalized with Np) as the dispersed phase. (c) Microscopic image and the schematic of the T-junction and a wiggled channel for rapid mixing of reagents online. (d) The high monodispersity of microfluidic droplets is demonstrated by the narrow size distribution. Reproduced with permission [124]. Copyright 2012, American Association for the Advancement of Science.

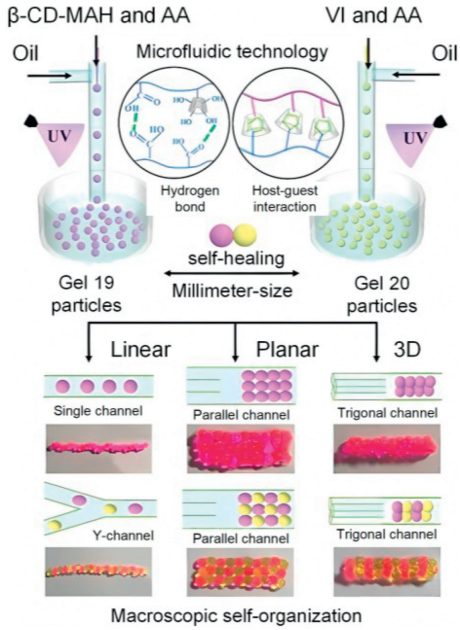

Fig. 20. Schematic diagram of a microfluidic-assisted SHDA for constructing linear 1D, planar 2D, and 3D macroscopic supramolecular assemblies. Reproduced with permission [125]. Copyright 2018, Wiley-VCH.

cell secretions and supramolecular agarose hydrogel were both encapsulated in uniform droplets, which were collected in the outlet channel and incubated at 37 °C for 18–24 h. After droplet separation and fluorescent labeling, single-cell protein secretion was detected with high throughput and signal enhancement. In this study, micro/nanofluidic droplets of supramolecular agarose hydrogel were successfully applied in protein analysis at the single-cell level.

The use of flow chemistry to construct supramolecular microcapsules offers similar advantages when constructing supramolecular hydrogels. In 2012, Abell and colleagues reported a one-step method for producing microcapsules, which were obtained by assembling each ligand at the interface of a droplet formed by the microfluidic chip [124]. Thus, the microcapsules had the combined advantages of microdroplet and supramolecular host-guest chemistry to enable both the quantitative loading of content and the stimulus-responsive release of the content. The host molecule chosen for this study was the cucurbit[8]uril (CB[8]) molecule, which can form dynamically stable complexes with the guest compound in water due to its large cavity (Fig. 19a). Gold nanoparticles (**17**) modified with electron-deficient methyl violet groups (**16a**) and thiol PEG derivatives (**16b**) together with water-soluble copolymers modified with electron-rich naphthalene groups (**18**) are the other two components of the microcapsules (Fig. 19b). A 1:1:1 ternary complex was formed in water, which was sufficient to accommodate methyl viologen and naphthofen. Each of the three components was injected from three injection ports into a microfluidic device with a simple T-shaped geometry, as shown in Fig. 19c. After the injection of these three components, the vertically injected fluorine oil generated shear force and reduced the interfacial energy, causing the colloidal particles contained in the aqueous phase to aggregate and form supramolecular microcapsules based on ternary host-guest complexes at the interface between the immiscible solution bodies. Stable microcapsules with hollow interiors were isolated within several minutes after dehydration. The encapsulation of specific compounds was achieved by changing the composition of the continuous phase. The release of the encapsulated material was achieved by stimulation since the microcapsules formed through host-guest interactions. Based on this principle, supramolecular polymers of different components at the interface of droplets were also produced, which provides a classical approach for designing and constructing supramolecular capsules.

Based on the above micro/nanofluidic techniques, various elegant macroscopic supramolecular assemblies of microspheres have been developed. In 2018, Chen *et al.* synthesized self-healing supramolecular hydrogel microspheres using micro/nanofluidic techniques, where gel **19** was formed by hydrogen bonding of carboxyl groups and β-cyclodextrin (β-CD), and gel **20** was formed by host-guest interaction between β-CD and vinyl imidazole (Fig. 20) [125]. By precisely controlling the flow rate and reaction time in different micro/nanochannels, uniform-sized microspheres that exhibited good self-healing ability through hydrogen bonding and host-guest interactions were obtained based on a self-healing-driven assembly (SHDH) strategy between the microspheres. Notably, linear one-dimensional (1D) and planar two-dimensional (2D) macroscopic supramolecular assemblies were constructed between the microspheres in just 5 s, and three-dimensional (3D) macroscale supramolecular assemblies were obtained within 5 min by continuously assembling the planar structure. This study provides a novel and efficient method for constructing supramolecular functional assemblies with macroscopic multidimensions.

Based on the precise regulation of the microstructure through flow chemistry, it is feasible to construct macroscopic MOF structures with various dimensions, such as hollow fibers or membranes. In 2014, Nair and colleagues developed a unique micro/nanofluidic chip to precisely control the macroscopic structure of MOF membranes [126]. These MOF membranes were considered 0D supramolecular assemblies with hollow tubular structures. Using a two-solvent interfacial method with the micro/nanofluidic chip, ZIF-8 membranes were formed *in situ* (Fig. 21a). They utilized polymeric hollow fibers as the support material at the dual-solvent interface, with a dilute Zn^{2+} ion and 1-octanol solution on the upper layer of the fiber and a high-concentration methylimidazole ligand aqueous solution on the lower layer of the fiber. At a low flow rate of 10 μL/h, due to the small volume (1.5 μL)

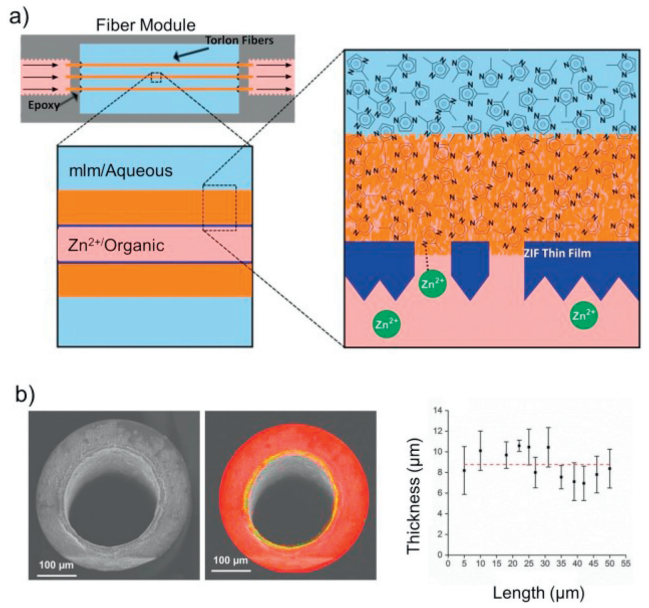

Fig. 21. (a) Schematic representation of the interfacial microfluidic membrane processing (IMMP) approach for forming MOF membranes in hollow fibers. (b) Cross-sectional SEM image, EDX characterization (EDX elemental maps of carbon (red) and superimposed zinc (green) showing the localization of the ZIF-8 membrane to the inner surface of the fiber) and thickness of the ZIF-8/hollow fiber membrane. Reproduced with permission [126]. Copyright 2014, American Association for the Advancement of Science.

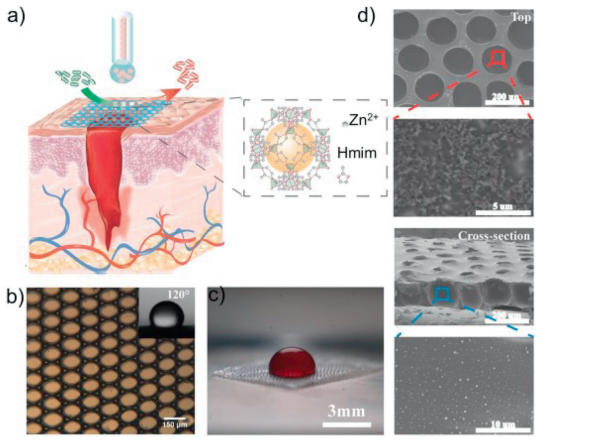

Fig. 22. (a) Schematic diagram of the fabrication of a ZIF-8@PVA hydrogel membrane by a microfluidic approach and the application of the hydrogel membrane in wound healing. (b) Microscopic optical image of the membrane with uniform pores. (c) Optical image of a drop of blood on the hydrogel membrane. (d) SEM images of the hydrogel membrane from a top view and cross-sectional view. Reproduced with permission [133]. Copyright 2020, Wiley-VCH.

of the polymeric hollow fibers and the lack of metal ion supplementation, ZIF-8 crystallization occurred in static growth phases, and the formed ZIF-8 membranes were inhomogeneous and dense. However, under continuous flow at a higher flow rate, the ZIF-8 thin membrane (approximately 2 μm) rapidly formed into a homogeneous and dense structure. This was due to the effect of hindering crystallization by the formed membrane, and the defects in the middle of the membrane preferentially continued to crystallize. Under static crystallization conditions, SEM and EDX characterization confirmed that the thickness of the ZIF-8 thin membrane increased, with a maximum thickness of approximately 9 μm (Fig. 21b). Gas adsorption experiments showed that this ZIF-8 membrane formed in polymeric hollow fibers by continuous flow exhibited excellent gas separation properties, with H_2/C_3H_8 separation ratios of up to 370 and C_3H_6/C_3H_8 separation ratios of up to 12.

In recent years, there has been a growing interest in using supramolecular hydrogels as membranes for wound treatment [127–129]. Given the respective advantages of supramolecular hydrogel "soft" materials and MOF "hard" materials, the development of wound treatment materials with antibacterial activity is of great significance [130]. MOFs have been proven to have excellent antibacterial properties and the ability to sustainably release antibacterial active species, such as metal ions and antibacterial drug molecules [131,132].

In 2020, Kong and colleagues reported the preparation of a porous MOF@supramolecular hydrogel membrane, where a two-dimensional porous supramolecular hydrogel loaded with MOFs was prepared using droplet-based micro/nanofluidic techniques [133]. The researchers used two known porous materials, ZIF-8 and polyvinyl alcohol (PVA) supramolecular hydrogel, to produce the ZIF-8@PVA supramolecular hydrogel membrane. The membrane was formed by collecting uniform oil-in-water droplets (PVA and ZIF-8 as the water phase, silicone oil as the oil phase) using a micro/nano fluidic system (Fig. 22a). After water evaporation and removal of the silicone oil, a porous MOF@PVA supramolecular hydrogel membrane was obtained (Figs. 22b–d). Microscopic optical images showed that the composite membrane material had uniform voids, and SEM images demonstrated that ZIF-8 was successfully loaded inside the membrane. Furthermore, the ZIF-8@PVA supramolecular hydrogel membrane was analyzed for biocompatibility and submitted to wound pathology testing and was found to not only inhibit the attachment of harmful microbes but also effectively deliver and release the antibacterial drug to wounded sites. Therefore, this composite membrane material has great potential as a wound dressing material with antibacterial activity.

Conductive MOFs represent a significant class of functionalized MOFs with potential applications in conduction and sensing [134]. To meet the demanding requirements of these applications, MOF macrostructures (membranes) need to possess specific features, such as a low thickness, uniform composition, and high density [135]. One of the most widely studied conductive MOFs is Ni_3(hexaiminotriphenylene)$_2$ ($Ni_3(HITP)_2$), which was found to exhibit high electrical conductivity (4–50 S/cm). While previous reports have discussed the synthesis of $Ni_3(HITP)_2$ membranes through solvothermal or on-substrate interface synthesis methods, a recent study by Park and coworkers in 2022 utilized micro/nanofluidic techniques to produce a highly transparent and flexible two-dimensional conductive MOF membrane (Fig. 23a) [136].

In their study, the authors employed a special dendritic chip, wherein metal salts and ligands were injected into a Y-shaped channel and rapidly mixed in an X-mixing channel to generate a large number of micro/nanodroplets in a dendritic channel. Combined with a rapid crystal synthesis process, this approach resulted in the formation of a high-quality, uniform $Ni_3(HITP)_2$ membrane on the substrate, as confirmed by SEM and PXRD data analysis. The $Ni_3(HITP)_2$ membrane prepared by micro/nanofluidic techniques exhibited high transparency (88.8%) and conductivity (up to 37.1 S/cm). Moreover, subsequent gas-sensing resistance experiments demonstrated excellent H_2S sensing performance, with the response time of this membrane being 30 times faster than that of $Ni_3(HITP)_2$ bulk (Fig. 23b). Overall, the $Ni_3(HITP)_2$ membrane synthesized using micro/nanofluidic techniques showed exceptional sensing performance and flexibility. The authors also integrated this $Ni_3(HITP)_2$ membrane into a face mask (Fig. 23c), which proved that this material had great potential for sensing and wearable devices.

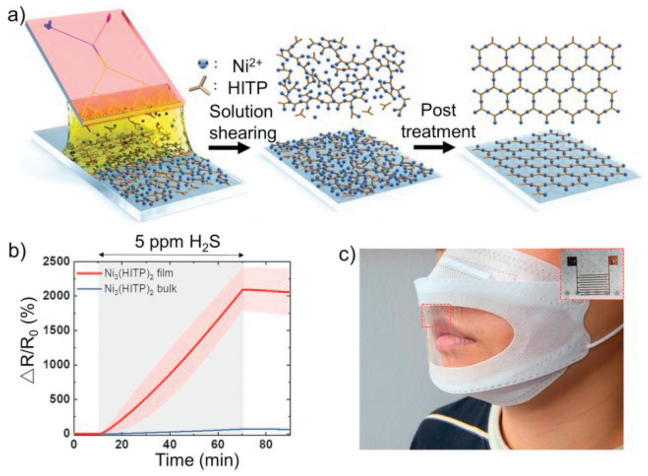

Fig. 23. (a) Schematic of MOF ($Ni_3(HITP)_2$) thin-film processing using a microfluidic-based solution shearing and postsynthesis process. (b) Dynamic response traces of $Ni_3(HITP)_2$ film and bulk upon exposure to 5 ppm H_2S. (c) Optical image of a face mask with integrated $Ni_3(HITP)_2$-based gas sensors. Reproduced with permission [136]. Copyright 2022, Wiley-VCH.

5. Conclusion

In summary, a variety of supramolecular assemblies with various structures have been developed using flow chemistry. For several decades, detailed studies on various supramolecular assemblies, such as macrocycles, cages, MOFs, COFs, and supramolecular hydrogels, have been conducted. Compared to traditional preparation methods, which often require harsh reaction conditions, such as anhydrous, oxygen-free, high-temperature, and high-pressure conditions, flow chemistry preparation methods cannot only allow milder synthesis conditions but also improve reaction efficiency and allow the ultrafast preparation of supramolecular assemblies. With this preparation method, supramolecular assemblies with high crystallinity, high particle size monodispersity, good stability, and high space-time yield can be synthesized in just a few seconds. In addition, micro/nanofluidic methods can allow the shape and composition of supramolecular assemblies to be precisely controlled to meet various application requirements.

The use of flow chemistry techniques for the preparation of supramolecular assemblies has been proven to be an excellent choice. Although the flow chemical synthesis of microscale and macroscale supramolecular assemblies has been greatly developed, the synthesis of nanoscale supramolecular assemblies using flow chemistry techniques is still limited. Furthermore, the synthesis of supramolecular assembly materials with more complex structures and diverse compositions, such as cage-coated nanoparticles, MOF crystals with core-shell structures, and MOF-enzyme complexes, still needs to be explored in depth. In subsequent studies, scientists ought to advance the integration of flow chemistry with photochemistry, microwave reactions, or more targeted synthetic methodologies to develop more versatile and accurate approaches for constructing supramolecular assemblies. These efforts should be directed toward not only the examination of the manifold properties of supramolecular assemblies but also toward improving the corresponding synthetic strategies. Based on the first proposed supramolecular flow chemistry herein, we believe that it will not only promote the development of supramolecular chemistry but also flow chemistry, more likely to promote the development of new cross-fields. The integration of principles and technologies from diverse fields into flow chemistry, coupled with in-depth interdisciplinary research, will further advance the field of supramolecular flow chemistry.

Declaration of competing interest

The authors declare that they have no known competing financial interests or personal relationships that could have appeared to influence the work reported in this paper.

Acknowledgments

This work was supported by the National Nature Science Foundation of China (Nos. 22107028 and 22103062), Program of Shanghai Outstanding Academic Leaders (No. 21XD1421200), Science and Technology Commission of Shanghai Municipality (No. 22JC1403900).

References

[1] E. Gazit, Nat. Chem. 2 (2010) 1010–1011.
[2] Y. Wang, Y. Qin, X. Zhao, et al., Chin. Chem. Lett. 34 (2023) 107576.
[3] P. Jia, L. Xu, Y. Hu, et al., J. Am. Chem. Soc. 143 (2021) 399–408.
[4] R. Chakrabarty, P.S. Mukherjee, P.J. Stang, Chem. Rev. 111 (2011) 6810–6918.
[5] Y. Hu, X. Hao, L. Xu, et al., J. Am. Chem. Soc. 142 (2020) 6285–6294.
[6] L. Chen, S. Chen, Y. Qin, et al., J. Am. Chem. Soc. 140 (2018) 5049–5052.
[7] Y. Qin, Y. Zhang, G. Yin, Chin. J. Chem. 37 (2019) 323–329.
[8] P. Jia, Y. Hu, Z. Zeng, et al., Chin. Chem. Lett. 34 (2023) 107511.
[9] X. Ji, M. Ahmed, L. Long, et al., Chem. Soc. Rev. 48 (2019) 2682–2697.
[10] S.D. Appavoo, S. Huh, D.B. Diaz, et al., Chem. Rev. 119 (2019) 9724–9752.
[11] S. Zhong, L. Zhu, S. Wu, et al., Chin. Chem. Lett. 34 (2023) 108124.
[12] H. Wang, Y. Jin, N. Sun, et al., Chem. Soc. Rev. 50 (2021) 8874–8886.
[13] E.G. Percástegui, T.K. Ronson, J.R. Nitschke, Chem. Rev. 120 (2020) 13480–13544.
[14] R. Saha, B. Mondal, P.S. Mukherjee, Chem. Rev. 122 (2022) 12244–12307.
[15] L. Feng, K.Y. Wang, G.S. Day, et al., Chem. Rev. 120 (2020) 13087–13133.
[16] X. Xiao, L. Zou, H. Pang, et al., Chem. Soc. Rev. 49 (2020) 301–331.
[17] B. Gui, G. Lin, H. Ding, et al., Acc. Chem. Res. 53 (2020) 2225–2234.
[18] X. Li, P. Yadav, K.P. Loh, Chem. Soc. Rev. 49 (2020) 4835–4866.
[19] B. Hu, C. Owh, P.L. Chee, et al., Chem. Soc. Rev. 47 (2018) 6917–6929.
[20] E.A. Appel, J. del Barrio, X.J. Loh, et al., Chem. Soc. Rev. 41 (2012) 6195–6214.
[21] A. Kumar, S.S. Sun, A.J. Lees, Coordin. Chem. Rev. 252 (2008) 922–939.
[22] S. Shinoda, Chem. Soc. Rev. 42 (2013) 1825–1835.
[23] M.D. Ward, Chem. Soc. Rev. 26 (1997) 365–375.
[24] H.Q. Peng, L.Y. Niu, Y.Z. Chen, et al., Chem. Rev. 115 (2015) 7502–7542.
[25] Y. Wang, Q. Zhou, X. He, et al., Chin. Chem. Lett. 33 (2022) 1613–1618.
[26] J. Li, P.M. Bhatt, J. Li, et al., Adv. Mater. 32 (2020) 2002563.
[27] J.R. Li, R.J. Kuppler, H.C. Zhou, Chem. Soc. Rev. 38 (2009) 1477–1504.
[28] C.M. Hong, R.G. Bergman, K.N. Raymond, et al., Acc. Chem. Res. 51 (2018) 2447–2455.
[29] J. Liu, L. Chen, H. Cui, et al., Chem. Soc. Rev. 43 (2014) 6011–6061.
[30] S. Rojas, A. Arenas-Vivo, P. Horcajada, Coordin. Chem. Rev. 388 (2019) 202–226.
[31] M.J. Webber, R. Langer, Chem. Soc. Rev. 46 (2017) 6600–6620.
[32] K. Zhang, Q. Feng, Z. Fang, et al., Chem. Rev. 121 (2021) 11149–11193.
[33] B. Huang, X. Liu, G. Yang, et al., CCS Chem. 4 (2021) 2090–2101.
[34] D.P. Dubal, N.R. Chodankar, D.H. Kim, et al., Chem. Soc. Rev. 47 (2018) 2065–2129.
[35] Q.Y. Xu, Z. Tan, X.W. Liao, et al., Chin. Chem. Lett. 33 (2022) 22–32.
[36] C. Piguet, J.C.G. Bünzli, Chem. Soc. Rev. 28 (1999) 347–358.
[37] B.J. Holliday, C.A. Mirkin, Angew. Chem. Int. Ed. 40 (2001) 2022–2043.
[38] Z. Xu, X. Huang, X. Han, et al., Chem 4 (2018) 1609–1628.
[39] X. Sun, M. Chwatko, D.H. Lee, et al., J. Am. Chem. Soc. 142 (2020) 3913–3922.
[40] B.A. Grzybowski, C.E. Wilmer, J. Kim, et al., Soft Matter 5 (2009) 1110–1128.
[41] A.I. Shallan, C. Priest, Chem. Eng. Process. 142 (2019) 107559.
[42] L. Buglioni, F. Raymenants, A. Slattery, et al., Chem. Rev. 122 (2022) 2752–2906.
[43] L. Li, Z. Gu, J.L. Zhou, et al., Chin. Chem. Lett. 32 (2021) 3416–3420.
[44] N. Cherkasov, P. Denissenko, S. Deshmukh, et al., Chem. Eng. J. 379 (2020) 122292.
[45] F. Zhao, D. Cambié, J. Janse, et al., ACS Sustain. Chem. Eng. 6 (2018) 422–429.
[46] J. Aubin, M. Ferrando, V. Jiricny, Chem. Eng. Sci. 65 (2010) 2065–2093.
[47] S. Wang, R. Zhou, Y. Hou, et al., Chin. Chem. Lett. 33 (2022) 3650–3656.
[48] L. Tamborini, P. Fernandes, F. Paradisi, et al., Trends Biotechnol. 36 (2018) 73–88.
[49] Z. Wang, Y. Zhou, M. Chen, Chin. J. Chem. 40 (2022) 285–296.
[50] J.A. Lv, Y. Liu, J. Wei, et al., Nature 537 (2016) 179–184.
[51] S. Feng, C. Pan, H. Ye, et al., Small 19 (2023) 2207383.
[52] F.J. Agostino, S.N. Krylov, Trends Anal. Chem. 72 (2015) 68–79.
[53] Q. Zhang, S. Feng, W. Li, et al., Angew. Chem. Int. Ed. 60 (2021) 8483–8487.
[54] P.S. Dittrich, A. Manz, Nat. Rev. Drug Discov. 5 (2006) 210–218.
[55] D. Hess, T. Yang, S. Stavrakis, Anal. Bioanal. Chem. 412 (2020) 3265–3283.
[56] S. Daniel, M.K. Chaudhury, P.G. de Gennes, Langmuir 21 (2005) 4240–4248.
[57] Z. Liu, J. Zhu, C. Peng, et al., React. Chem. Eng. 4 (2019) 1699–1720.
[58] J. Zhang, J. Chen, S. Peng, et al., Chem. Soc. Rev. 48 (2019) 2566–2595.
[59] X. Sun, Q. Wu, W. Li, et al., Chin. Chem. Lett. 33 (2022) 2697–2700.

[60] S. Sevim, A. Sorrenti, C. Franco, et al., Chem. Soc. Rev. 47 (2018) 3788–3803.
[61] J. Li, J. Pan, W. Yin, et al., Chin. Chem. Lett. 34 (2023) 108049.
[62] R.M. Myers, D.E. Fitzpatrick, R.M. Turner, et al., Chem. Eur. J. 20 (2014) 12348–12366.
[63] B. Qin, Z. Yin, X. Tang, et al., Prog. Polym. Sci. 100 (2020) 101167.
[64] L. Jean-Marie, Rep. Prog. Phys. 67 (2004) 249.
[65] J. Sui, J. Yan, D. Liu, et al., Small 17 (2021) 2104166.
[66] Z. Ye, Z. Yang, L. Wang, et al., Angew. Chem. Int. Ed. 58 (2019) 12519–12523.
[67] M. Han, R. Michel, B. He, et al., Angew. Chem. Int. Ed. 52 (2013) 1319–1323.
[68] Z. Zhang, Z. Zhao, L. Wu, et al., J. Am. Chem. Soc. 142 (2020) 2592–2600.
[69] T.L. Mako, J.M. Racicot, M. Levine, Chem. Rev. 119 (2019) 322–477.
[70] D. Zhang, W. Yu, S. Li, et al., J. Am. Chem. Soc. 143 (2021) 1313–1317.
[71] W. Cullen, M.C. Misuraca, C.A. Hunter, et al., Nat. Chem. 8 (2016) 231–236.
[72] B.D. Egleston, M.C. Brand, F. Greenwell, et al., Chem. Sci. 11 (2020) 6582–6589.
[73] H. Kim, H.J. Lee, D.P. Kim, Angew. Chem. Int. Ed. 55 (2016) 1422–1426.
[74] C.D. Jones, L.J. Kershaw Cook, D. Marquez-Gamez, et al., J. Am. Chem. Soc. 143 (2021) 7553–7565.
[75] G. Montà-González, F. Sancenón, R. Martínez-Máñez, et al., Chem. Rev. 122 (2022) 13636–13708.
[76] H. Duan, F. Cao, M. Zhang, et al., Chin. Chem. Lett. 33 (2022) 2459–2463.
[77] M. Kitchin, K. Konstas, C.J. Sumby, et al., Chem. Commun. 51 (2015) 14231–14234.
[78] M.E. Briggs, A.G. Slater, N. Lunt, et al., Chem. Commun. 51 (2015) 17390–17393.
[79] Z. Shi, Y. Tao, J. Wu, et al., J. Am. Chem. Soc. 142 (2020) 2750–2754.
[80] Q. Fang, S. Gu, J. Zheng, et al., Angew. Chem. Int. Ed. 53 (2014) 2878–2882.
[81] Y. Ye, S. Xian, H. Cui, et al., J. Am. Chem. Soc. 144 (2022) 1681–1689.
[82] H.L. Qian, C.X. Yang, X.P. Yan, Nat. Commun. 7 (2016) 12104.
[83] Y. Wang, H. Liu, Q. Pan, et al., J. Am. Chem. Soc. 142 (2020) 5958–5963.
[84] T. He, S. Chen, B. Ni, et al., Angew. Chem. Int. Ed. 57 (2018) 3493–3498.
[85] Y. Xin, S. Peng, J. Chen, et al., Chin. Chem. Lett. 31 (2020) 1448–1461.
[86] H.L. Zhou, J. Bai, X.Y. Tian, et al., Chin. J. Chem. 39 (2021) 2718–2724.
[87] M. Wu, L. Xia, Y. Li, et al., Chin. Chem. Lett. 33 (2022) 497–500.
[88] M. Faustini, J. Kim, G.Y. Jeong, et al., J. Am. Chem. Soc. 135 (2013) 14619–14626.
[89] L. Paseta, B. Seoane, D. Julve, et al., ACS Appl. Mater. Interfaces 5 (2013) 9405–9410.
[90] A. Polyzoidis, T. Altenburg, M. Schwarzer, et al., Chem. Eng. J. 283 (2016) 971–977.
[91] Y. Peng, W.K. Wong, Z. Hu, et al., Chem. Mater. 28 (2016) 5095–5101.
[92] C. Echaide-Górriz, C. Clément, F. Cacho-Bailo, et al., J. Mater. Chem. A 6 (2018) 5485–5506.
[93] C. Crivello, S. Sevim, O. Graniel, et al., Mater. Horiz. 8 (2021) 168–178.
[94] Y. Tanaka, S. Yamada, D. Tanaka, Chempluschem 86 (2021) 650–661.
[95] R. Ameloot, F. Vermoortele, W. Vanhove, et al., Nat. Chem. 3 (2011) 382–387.
[96] G.Y. Jeong, R. Ricco, K. Liang, et al., Chem. Mater. 27 (2015) 7903–7909.
[97] S. Wu, Z. Xin, S. Zhao, et al., Nano Res. 12 (2019) 2736–2742.
[98] C. Hu, Y. Bai, M. Hou, et al., Sci. Adv. 6 (2020) eaax5785.
[99] X. Dong, J. Yang, H. Wang, et al., Chin. J. Chem. 40 (2022) 1171–1176.
[100] D. Rodríguez-San-Miguel, A. Abrishamkar, J.A.R. Navarro, et al., Chem. Commun. 52 (2016) 9212–9215.
[101] D. Witters, N. Vergauwe, R. Ameloot, et al., Adv. Mater. 24 (2012) 1316–1320.
[102] N. Vogel, M. Retsch, C.A. Fustin, et al., Chem. Rev. 115 (2015) 6265–6311.
[103] C.X. Zhao, A.P.J. Middelberg, Chem. Eng. Sci. 66 (2011) 1394–1411.
[104] Y. Shen, A. Levin, A. Kamada, et al., ACS Nano 15 (2021) 5819–5837.
[105] Q.H. Zhao, F.H. Cao, Z.H. Luo, et al., Angew. Chem. Int. Ed. 61 (2022) e202117500.
[106] Y.F. Li, Z. Li, Q. Lin, et al., Nanoscale 12 (2020) 2180–2200.
[107] X. Du, J. Zhou, J. Shi, et al., Chem. Rev. 115 (2015) 13165–13307.
[108] J. Omar, D. Ponsford, C.A. Dreiss, et al., Chem. Asian J. 17 (2022) e202200081.
[109] F. Trausel, F. Versluis, C. Maity, et al., Acc. Chem. Res. 49 (2016) 1440–1447.
[110] A. Döring, W. Birnbaum, D. Kuckling, Chem. Soc. Rev. 42 (2013) 7391–7420.
[111] X. Dou, N. Mehwish, C. Zhao, et al., Acc. Chem. Res. 53 (2020) 852–862.
[112] D.L. Taylor, Adv. Mater. 28 (2016) 9060–9093.
[113] C. Zhang, B. Wu, Y. Zhou, et al., Chem. Soc. Rev. 49 (2020) 3605–3637.
[114] Z. Wei, S. Wang, J. Hirvonen, et al., Adv. Healthc. Mater. 11 (2022) 2200846.
[115] L. Shang, Y. Cheng, Y. Zhao, Chem. Rev. 117 (2017) 7964–8040.
[116] J. Zhang, Y. Qin, Y. Ou, et al., Angew. Chem. Int. Ed. 61 (2022) e202206339.
[117] W. Yang, S. Feng, X. Zhang, et al., ACS Appl. Mater. Interfaces 13 (2021) 38722–38731.
[118] F. Sheehan, D. Sementa, A. Jain, et al., Chem. Rev. 121 (2021) 13869–13914.
[119] W. Chen, Y. Yang, C. Rinadi, et al., Lab Chip 9 (2009) 2947–2951.
[120] J.A. Foster, R.M. Parker, A.M. Belenguer, et al., J. Am. Chem. Soc. 137 (2015) 9722–9729.
[121] F. Zhu, Y. Ji, J. Deng, et al., Chin. Chem. Lett. 33 (2022) 2893–2900.
[122] Z. Wu, L. Lin, Chin. Chem. Lett. 33 (2022) 1752–1756.
[123] V. Chokkalingam, J. Tel, F. Wimmers, X. Liu, et al., Lab Chip 13 (2013) 4740–4744.
[124] J. Zhang, R.J. Coulston, S.T. Jones, et al., Science 335 (2012) 690–694.
[125] Q. Li, Y.W. Zhang, C.F. Wang, et al., Adv. Mater. 30 (2018) 1803475.
[126] A.J. Brown, N.A. Brunelli, K. Eum, et al., Science 345 (2014) 72–75.
[127] S. Khosravimelal, M. Mobaraki, S. Eftekhari, et al., Small 17 (2021) 2006335.
[128] Y. Liang, J. He, B. Guo, ACS Nano 15 (2021) 12687–12722.
[129] Y. Wang, L. Sun, G. Chen, et al., ACS Nano 17 (2023) 1437–1447.
[130] X. Liu, Y. Xiao, Z. Zhang, et al., Chin. J. Chem. 39 (2021) 3462–3480.
[131] R. Li, T. Chen, X. Pan, ACS Nano 15 (2021) 3808–3848.
[132] D. Han, X. Liu, S. Wu, Chem. Soc. Rev. 51 (2022) 7138–7169.
[133] X. Yao, G. Zhu, P. Zhu, et al., Adv. Funct. Mater. 30 (2020) 1909389.
[134] H.Y. Li, S.N. Zhao, S.Q. Zang, et al., Chem. Soc. Rev. 49 (2020) 6364–6401.
[135] S. Qiu, M. Xue, G. Zhu, Chem. Soc. Rev. 43 (2014) 6116–6140.
[136] T. Lee, J.O. Kim, C. Park, et al., Adv. Mater. 34 (2022) 2107696.